Supporting Information:

All geometry optimized structures and energy values are available from the authors upon request.

Table 1: Comparison of key bond distances and bond angles of *bis*-L complexes (L = 4-MeIm, NH3, 2-MeIm, *N*-MeIm, Im, and py) determined by X-ray crystallography to those optimized with B3LYP/6-31G(d) and B3LYP/cc-pVDZ.

		4-MeIm			NH_3			2-MeIm		
		exp	6-31G(d)	cc-pVDZ	exp	6-31G(d)	cc-pVDZ	exp	6-31G(d)	cc-pVDZ
Bond Distances (Å)	Co-O_{eq}	1.897	1.903	1.921	1.897	1.895	1.916	1.899	1.904	1.923
	Co-N_{eq}	1.899	1.921	1.930	1.889	1.916	1.928	1.904	1.921	1.931
	Co-N_{ax}	1.947	1.961	1.982	1.941	1.971	1.984	1.965	1.991	2.012
Bond Angles (degrees)	O_{eq}-Co-O_{eq}	83.1	85.2	85.7	84.3	85.4	85.8	85.3	87.7	87.9
	N_{eq}-Co-O_{eq}	95.1	94.5	94.2	94.9	94.3	94.1	94.4	93.7	93.5
	N_{eq}-Co-N_{eq}	86.8	85.8	85.9	85.9	86.1	85.9	85.8	85.0	85.0
	N_{eq}-Co-N_{ax}	90.8	91.5	91.4	91.6	92.6	92.5	90.3	91.2	91.2
	O_{eq}-Co-N_{ax}	89.2	88.5	88.6	88.3	87.4	87.4	89.7	88.8	89.2

		N-MeIm			Im			py		
		exp	6-31G(d)	cc-pVDZ	exp	6-31G(d)	cc-pVDZ	exp	6-31G(d)	cc-pVDZ
Bond Distances (Å)	Co-O_{eq}	1.900	1.903	1.921	1.885	1.902	1.920	1.904	1.899	1.917
	Co-N_{eq}	1.899	1.916	1.929	1.880	1.920	1.930	1.904	1.918	1.930
	Co-N_{ax}	1.941	1.961	1.978	1.931	1.963	1.980	1.959	1.993	2.014
Bond Angles (degrees)	O_{eq}-Co-O_{eq}	83.5	85.1	85.6	83.8	85.2	85.6	85.7	85.9	86.2
	N_{eq}-Co-O_{eq}	95.0	94.5	94.3	95.3	94.4	94.3	94.6	94.3	94.3
	N_{eq}-Co-N_{eq}	86.6	85.9	85.8	85.6	86.0	85.8	85.2	85.5	85.3
	N_{eq}-Co-N_{ax}	89.9	91.5	91.6	90.5	91.4	91.5	91.9	92.0	92.0
	O_{eq}-Co-N_{ax}	90.1	88.5	88.4	89.5	88.6	88.5	88.2	88.6	88.0

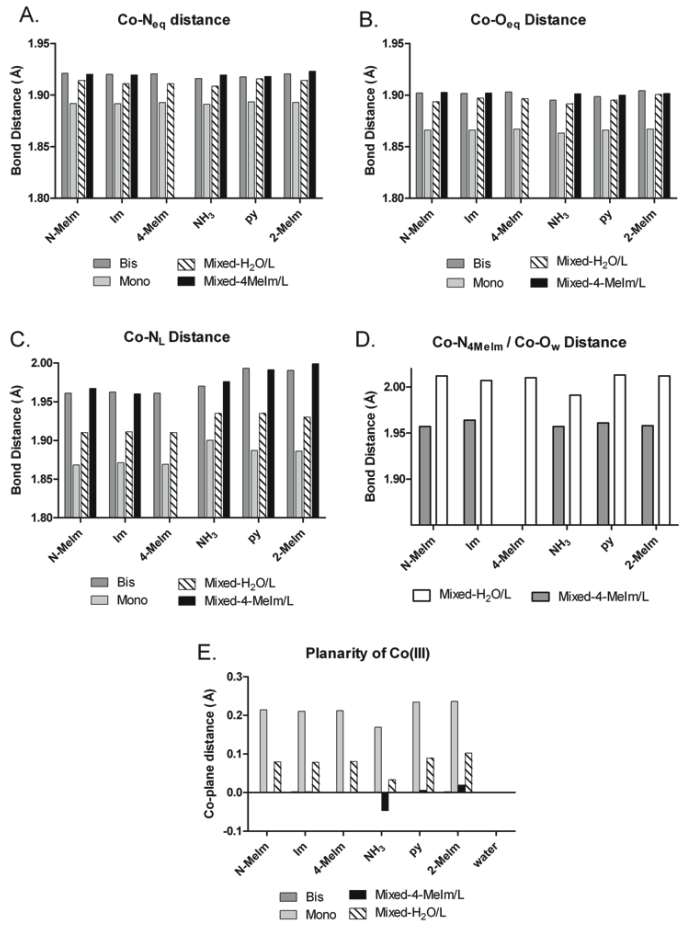

Figure SI-1: A) Co-N_{eq} B) Co-O_{eq} and C) Co-N_L distances for *bis*-L, *mono*-L, and *mixed*-4MeIm-L complexes, where L = N-MeIm, Im, 4-MeIm, NH_3, py, and 2-MeIm. The Co-O_{eq} and Co-N_{eq} distances are essentially independent of the identity of L, but are slightly shorter for the *mono*-L complexes than the *bis*-L or *mixed*-4-MeIm-L complexes. The Co-N_L distance shows only slightly more dependence on the axial ligand, but is more significantly shortened (~ 0.1 A) upon formation of the 5-coordinate *mono*-L species. D) Distance between Co(III) and the nitrogen of 4-MeIm or the oxygen of the water molecule for the *mixed*-4-MeIm/L and *mixed*-H_2O/L complexes, respectively. E) Displacement of Co(III) from the N_2O_2 plane. Note that the metal lies in the plane for all *bis* and *mixed*-4MeIm-L structures, but is pulled significantly toward the axial ligand in the *mono*-L complexes. All distances are reported as the average between equivalent atoms.

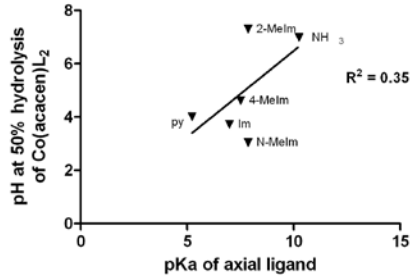

Figure SI-2: pH instability of $[Co(acacen)L_2]^+$ (measured as the pH at which 50% of the starting material has been hydrolyzed) versus pK_a of the axial ligand (data obtained from Part I). Both the pyridine and 2-MeIm complexes exhibit unexpectedly low pH stability for their pK_a values, while N-MeIm exhibits greater stability than expected. This indicates that pK_a of the axial ligand is not the only factor determining pH stability of these complexes.

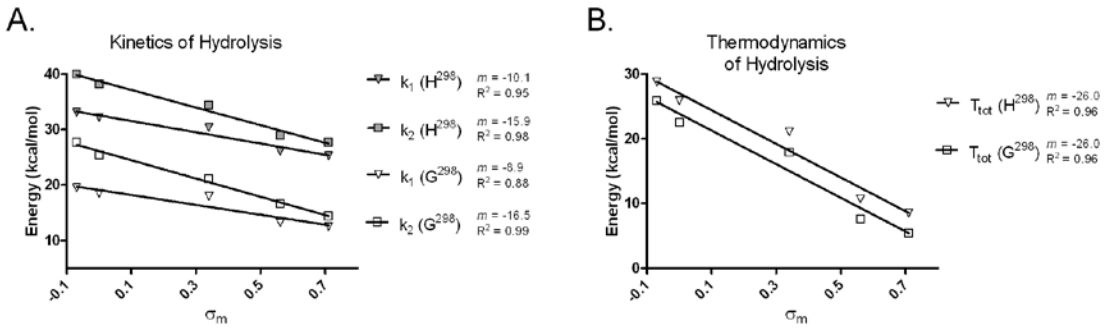

Figure SI-3: Correlation between the electron withdrawing capability of the substituent on the axial ligand and A) the kinetic barrier for ligand dissociation and B) the thermodynamic destabilization resulting from hydrolysis of Co(acacen)L_2. As the strength of the EWG increases, the activation barrier decreases while the thermodynamic destabilization that occurs as a result of hydrolysis decreases.

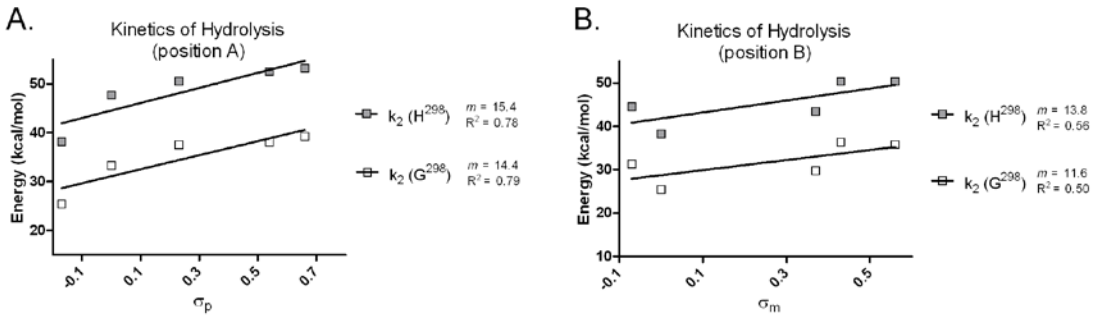

Figure SI-4: Correlation between the electron withdrawing capability of the substituent on the acacen ligand and the kinetics of ligand dissociation. If the substitution is made at position A, an increase in EWG is correlated to an increase in activation barrier. No such correlation exists if the substitution is made at position B.

Figures SI5 – SI9 were created using the results obtained with the cc-pVDZ basis set. These results show the same trends as those obtained with the 6-31G(d) basis set which were reported in the manuscript.

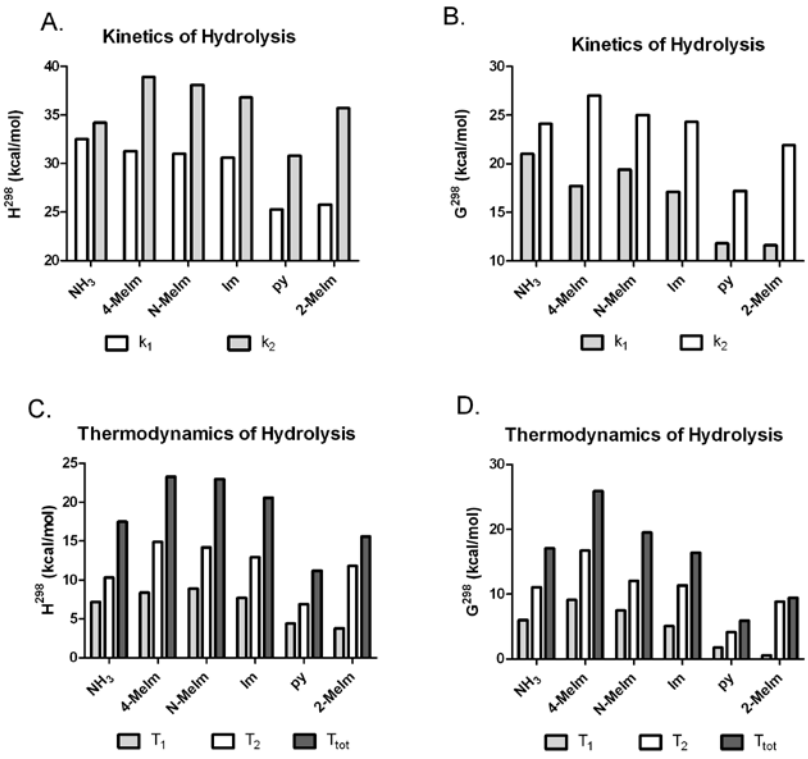

Figure SI-5: Kinetics and thermodynamics of hydrolysis.

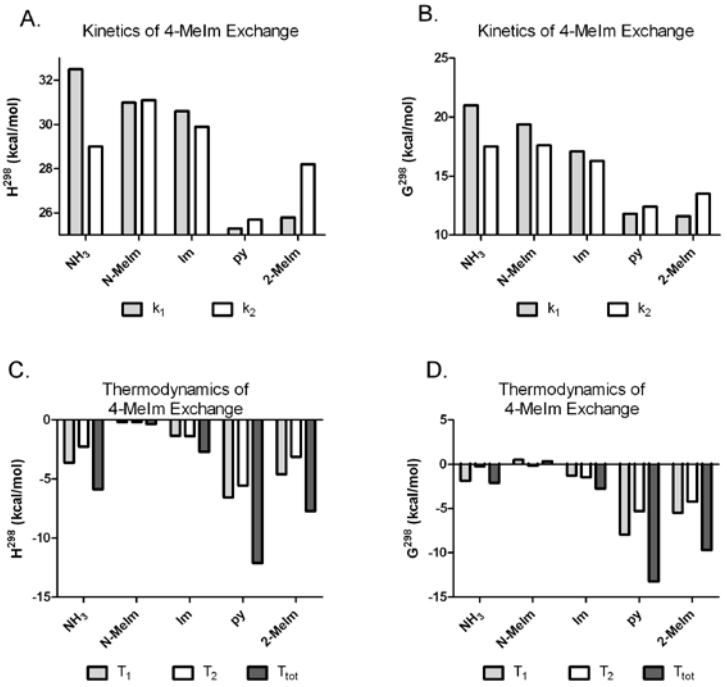

Figure SI-6: Kinetics and thermodynamics of ligand exchange with 4-MeIm.

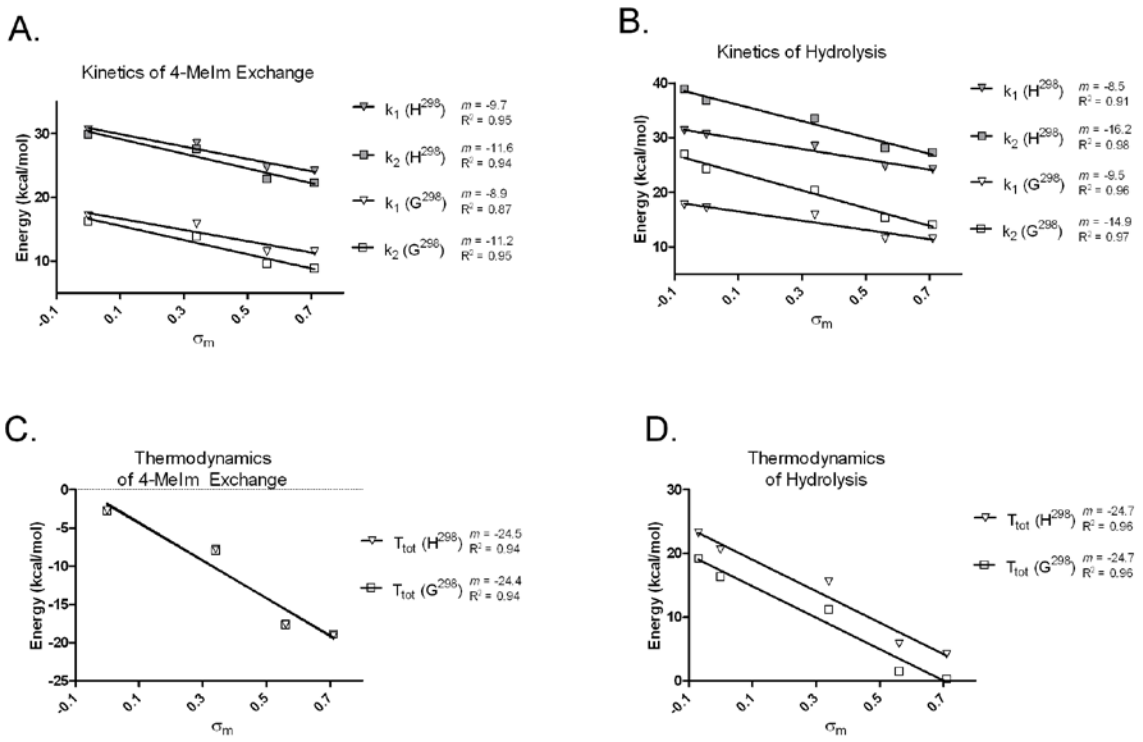

Figure SI-7: Correlation between kinetics and thermodynamics of ligand exchange/hydrolysis and the EW capability of substituents on the axial ligand.

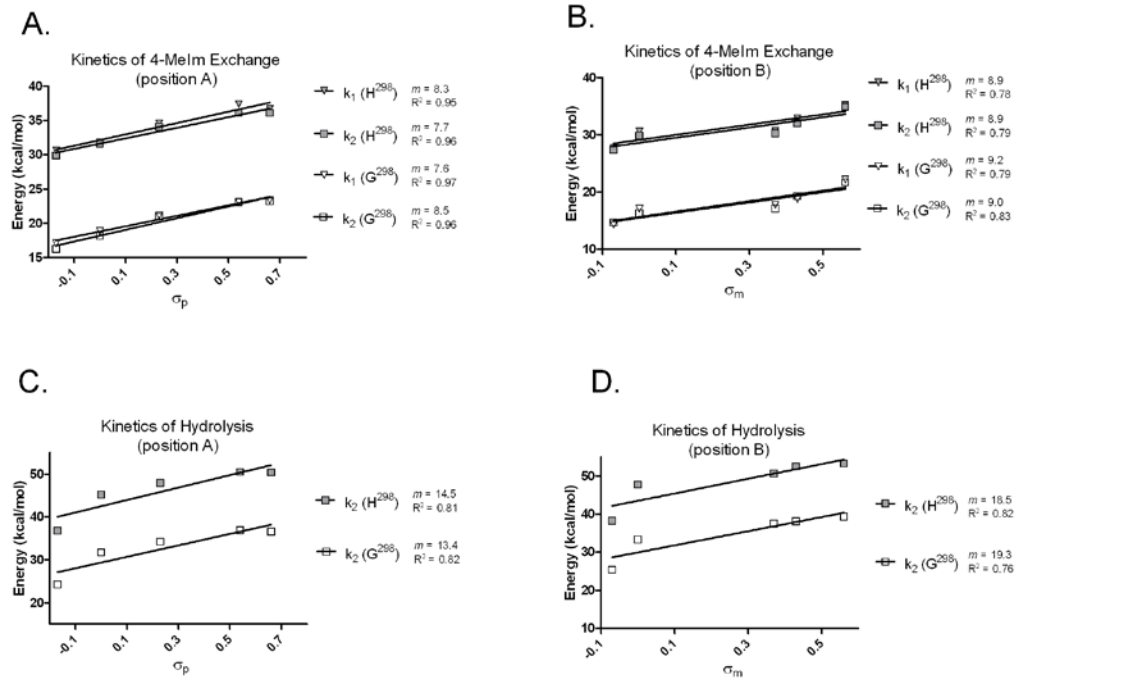

Figure SI-8: Correlation between kinetics of ligand exchange/hydrolysis and the EW capability of substituents on the A or B position of the acacen ligand.

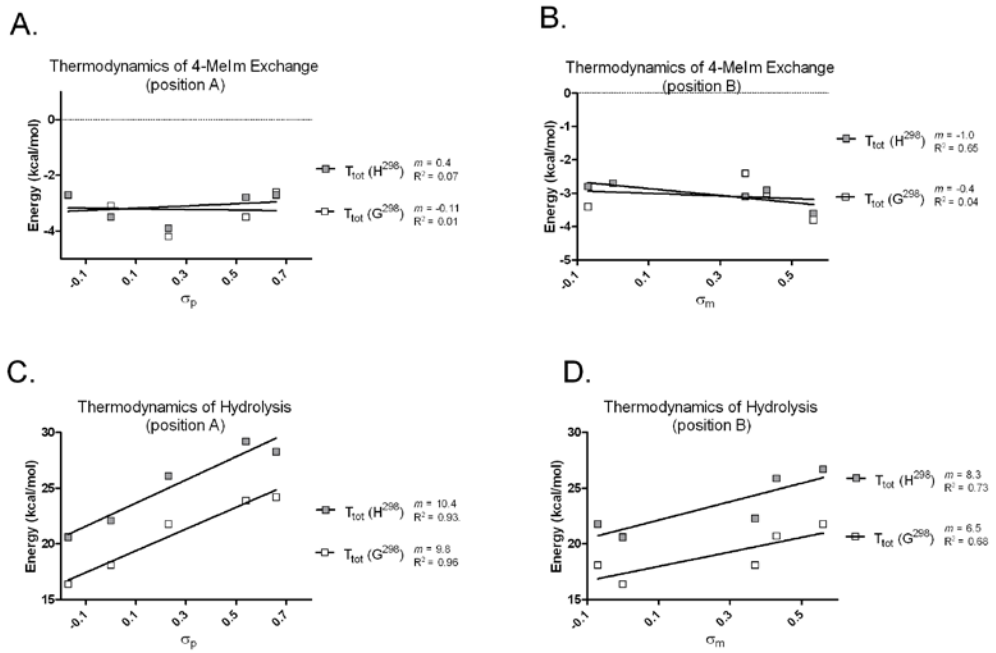

Figure SI-9: Correlation between thermodynamics of ligand exchange/hydrolysis and the EW capability of substituents on the A or B position of the acacen ligand.

Discussion of NBO results:

Orbital Interactions: NBO calculations indicate that the orbital interactions between the Co(III) center and the axial ligands are dominated by σ-donation from the lone pairs of the coordinating nitrogens into the unoccupied d_z^2 and 4*s* orbitals of the metal (Figure 8). Back-donation from the filled *d*-orbitals of the metal into the π^*-orbitals of the aromatic rings is negligible for all axial ligands examined in this study. (Donation from the metal into the N-H σ^*-bonds of the ammine ligands is also negligible). These results are to be expected given the location of imidazole and pyridine derivatives within the spectrochemical series.[44]

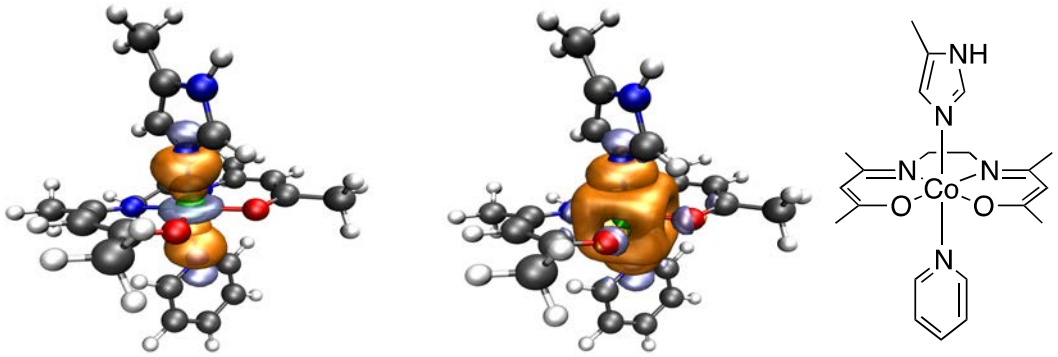

Figure SI-10: Orbital interactions between Co(III) and the axial ligands of the *mixed*-4-MeIm/py complex. The interactions are dominated by σ-donation from the lone pairs of the coordinating nitrogens into the unoccupied d_z^2 (left) and 4*s* (middle) orbitals. A schematic of the structures is shown on the right.

The strength of the σ-donor interaction is almost entirely independent of the axial ligand; the only exception being the *mixed*-4-MeIm/py complex, in which the Co-4MeIm interaction is slightly stronger (~ 7%) than the Co-py interaction. While this is a very minor difference, it is notable given that all other *mixed*-4-MeIm/L complexes exhibit the same degree of σ-donation for the two different ligands. Moreover, the *bis*-py complex exhibits the lowest activation barrier for ligand dissociation, suggesting that, for these types of complexes, py is a slightly weaker σ-donor than imidazole derivatives.